Wind and Structures, *Vol. 24, No. 1 (2017) 59-78*
DOI: https://doi.org/10.12989/was.2017.24.1.059

Non-stationary and non-Gaussian characteristics of wind speeds

Yi Hui*[1], Bo Li[2], Hiromasa Kawai[3] and Qingshan Yang[2]

[1]*Wind Engineering Research Center, College of civil engineering, Hunan University, Changsha, 410082 China*
[2]*Beijing's Key Laboratory of Structural Wind Engineering and Urban Wind Environment, School of civil engineering, Beijing Jiaotong University, Beijing, 100044, China*
[3]*School of Science and Engineering, Tokyo Denki University, Ishizaka, Hatoyama, Hikigun, Saitama 350-0394, Japan*

(Received March 1, 2016, Revised November 15, 2016, Accepted November 21, 2016)

Abstract. Non-stationarity and non-Gaussian property are two of the most important characteristics of wind. These two features are studied in this study based on wind speed records measured at different heights from a 325 m high meteorological tower during the synoptic wind storms. By using the time-frequency analysis tools, it is found that after removing the low frequency trend of the longitudinal wind, the retained fluctuating wind speeds remain to be asymmetrically non-Gaussian distributed. Results show that such non-Gaussianity is due to the weak-stationarity of the detrended fluctuating wind speed. The low frequency components of the fluctuating wind speeds mainly contribute to the non-zero skewness, while distribution of the high frequency component is found to have high kurtosis values. By further studying the decomposed wind speed, the mechanisms of the non-Gaussian distribution are examined from the phase, turbulence energy point of view.

Keywords: full scale measurement; synoptic wind storm; signal processing; time-frequency analysis

1. Introduction

The knowledge of characteristics of wind is the most basic and important aspect in wind engineering field. Thus, the full-scale wind field investigations become crucial for this purpose. The wind field of typhoon above high-rise buildings is one of the topics that researchers are interested in (Li, Xiao *et al*. 2005, Yi, Zhang *et al*. 2013). Hui, Larsen *et al.* (2009a, b) monitored the wind field around Stonecutters Bridge for 27 months. They studied the mean wind speeds, turbulence intensities, wind power spectra, and integral length scales, etc. which made important contributions for the design of Stonecutters Bridge. Toriumi, Katsuchi *et al.* (2000) measured the wind speeds on the Honshu-Shikoku Bridge and studied the spatial correlation of wind field in order to analyze the wind induced response of that bridge. Studies are also made on the wind speed data obtained from the 325 m meteorological tower in Beijing (Li, Zhi *et al*. 2010), to discuss the wind profile and related wind characteristics at 3 different heights of the tower.

Most of the studies on wind characteristics ignored the non-stationary and non-Gaussian

*Corresponding author, Dr., E-mail: alihui@hnu.edu.cn

http://www.techno-press.org/?journal=was&subpage=8 ISSN: 1226-6116 (Print), 1598-6225 (Online)

features of wind. With the development of analyzing techniques in wind engineering, more and more researchers are moving their focuses from the stationary Gaussian wind to the non-stationary and non-Gaussian wind (Kareem and Kijewski 2002, Kareem 2008, Kawai 2009, Huang, Huang *et al*. 2016, Tao, Wang *et al*. 2016). Balderrama, Masters *et al*. (2012) studied the peak factor of wind speed observed at 10 m above the ground during hurricanes, and proposed a method for estimating the peak factor of non-Gaussian wind speed. This change greatly improves the analysis method of the wind induced response of structures (Gong and Chen 2014, Hu, Xu *et al*. 2013).

However, many studies adopted the time-frequency analysis method to investigate the transient wind like downburst storm (Chen and Letchford 2005, Wang *et al*. 2013, Su, Huang *et al*. 2015). Only a few studies have focused on the non-stationary and non-Gaussian characteristics of synoptic wind speeds.

Xu and Chen (2004) tackled the non-stationary wind speed by using Empirical Mode Decomposition (EMD) technique. This method can successfully find the trend information from the wind speed records, and make the non-stationary data to be stationary by subtracting trend from original data. However, this study only addressed the low frequency trend's contribution to the non-stationarity and non-Gaussianity. Kitagawa and Nomura (2003) investigated the energy cascade of fluctuating wind speed through Discrete Wavelet Transformation (DWT) (Chui 1992), as the intermittency of turbulence energy of high frequency components can be well studied and simulated with the help of DWT.

It can be found that, the existing studies have only focused on one or two features of the wind speed. While a comprehensive analysis of characteristics of wind speed during the synoptic storm are still needed. In this study, existing analysis methods for non-stationarity are firstly introduced and discussed, then a more detailed discussion on the fluctuating wind speed is presented. The non-stationary and non-Gaussian characteristics of wind speed are studied by the means of time-frequency analysis. The mechanism of the non-stationary and non-Gaussian characteristics of synoptic wind at various heights are studied. The wind speed data used for the analysis was obtained from a 325 m high meteorological tower with more than one year's continuous observation.

2. Introduction of field measurement

The 325 m high meteorological tower, which is a guyed tower with regular triangle cross section, is located at the north center of Beijing, China. Fig. 1 shows the picture of the tower and the definition of wind direction. There is almost no high rise structures within 1 km range of the tower, except that some residential buildings, about 60 m high, are located 100 m from the tower in the south direction. Nine three-channel ultrasonic anemometers are mounted at nine different heights along the tower, which are 8 m, 16 m, 32 m, 47 m, 64 m, 80 m, 140 m, 200 m, and 280 m respectively. To check the reliability of instrument, the measured wind speeds at each height are firstly averaged within each 10 min and compared with the cup-type anemometers. Moreover, two ultrasonic anemometers are mounted at 16 m and 32 m, respectively, for validating the measured fluctuating speeds. Thus, the fidelity of instruments is well examined before further analysis. To avoid the interference effects of the tower on wind, anemometers are fixed 1.5 m away from the tower in the north which is in the upwind direction of the tower during dominant synoptic wind in Beijing during winter and spring. All these anemometers continuously collect wind speed data simultaneously with a sampling frequency of 10 Hz. The 3 instantaneous wind speed component in

orthogonal directions are indicated by UN(t)—North-South direction(positive when wind comes from north), UE(t)—East-West direction(positive when wind comes from east), UV(t)—vertical direction. Wind speed data used in this study were recorded from Nov. 19th, 2012 to Feb. 28th, 2014. Totally 53 independent relatively strong wind storm data are selected in this period, with 44 synoptic storms in winter and spring, and 9 summer thunder storms.

Fig. 2 shows a typical 10 min mean wind speeds and directions time series of the synoptic storms in winter and spring. Mean wind speed and direction are obtained based on the following equations

$$\overline{U} = \sqrt{\overline{U}_E^2 + \overline{U}_N^2} \tag{1}$$

$$\theta = \begin{cases} \cos^{-1}\dfrac{\overline{U}_N}{\overline{U}} & (\overline{U}_E > 0) \\ 360 - \cos^{-1}\dfrac{\overline{U}_N}{\overline{U}} & (\overline{U}_E < 0) \end{cases} \tag{2}$$

where, $\overline{U}_E = \dfrac{1}{T}\int_0^T U_E(t)dt$, $\overline{U}_N = \dfrac{1}{T}\int_0^T U_N(t)dt$,and T is 10 min.

Such storms usually have relative long period of about up to several days. The wind direction of the whole storm remains relatively stable. The storm shown in Fig. 2 is from 11:10, Dec. 25th, 2013 to 23:10, Dec. 26th, 2013, lasting for 36 hours. The maximum 10 min mean wind speed at 280 m is 22.7 m/s which is the highest in the whole 1 year observation period. Fig. 2(b) shows the 10 min mean wind direction. It can be seen that the wind directions at all 4 different heights remain stable.

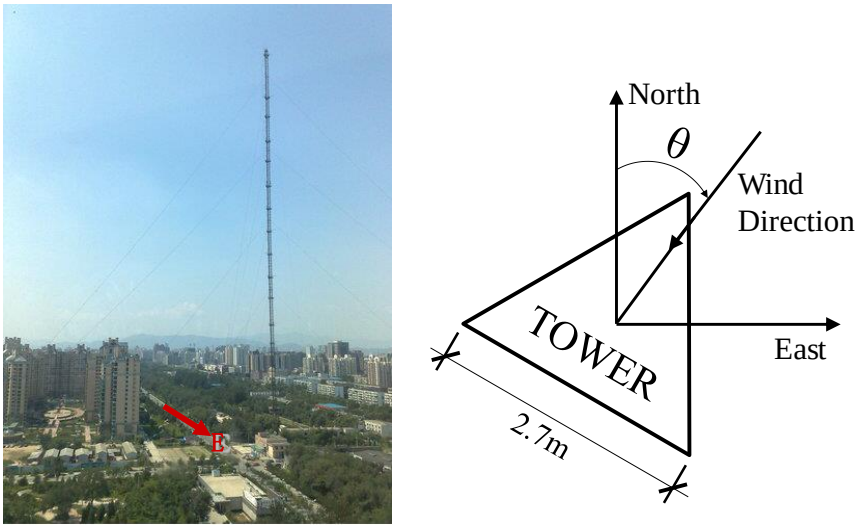

Fig. 1 Meteorological tower and definition of wind direction

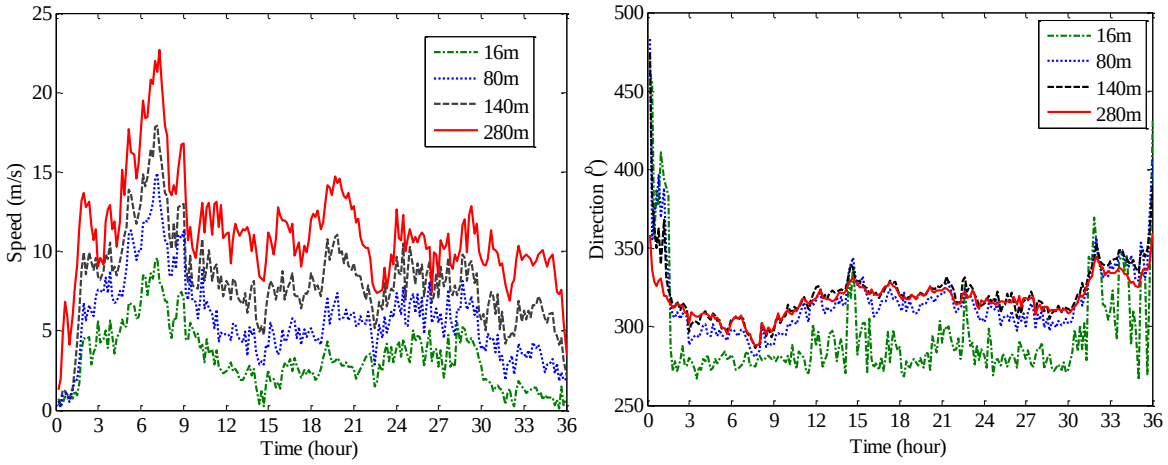

(a) Wind speed (b) Wind direction

Fig. 2 10 min mean wind speed and directions of the storm Dec. 25th, 2013 at the 4 heights

3. Existing fluctuating wind speeds analysis methods

3.1 Constant mean approach

In this approach, the longitudinal wind speeds is divided into two parts, which can be expressed as

$$U(t) = \overline{U} + u(t) \tag{3}$$

where $\overline{U}$ is the constant mean wind speed for a time interval and is usually taken as 10 min or 1h, and $u(t)$ is the fluctuating component (AIJ 2004; NRS 2005). $u(t)$ is assumed to be a zero-mean stationary random process following the Gaussian distribution. However, with more and more field data collected, this assumption is found hardly satisfied.

Every hour's wind speeds from 4th to 30th hour at 280 m high described above undergoes the Mann-Kendall test (Hamed and Rao 1998), which is a non-parametric monotonic trend test method. Results show that 24 out of 27 samples are examined with trend. Such results indicate that most of the observed wind speeds of this storm cannot satisfy this assumption with even the 1st order stationarity (constant mean process).

3.2 Time-varying trend approach

Based on the fact introduced in Sec. 3.1, an alternative method is introduced to solve the non-stationarity problem of the fluctuating component $U_{dt}(t)$. In this approach, wind speed is described as the sum of a deterministic trend component and a fluctuating component that is again assumed to be a zero-mean stationary Gaussian random process (Farge 1992, Gurley and Kareem 1999, Hayashi 1994, Kareem and Kijewski 2002, Xu and Chen 2004).

$$U(t) = U_{tr}(t) + U_{dt}(t) \tag{4}$$

where $U_{tr}(t)$ the time-varying trend component, $U_{dt}(t)$ is the detrended fluctuating component. Discrete Wavelet Transform(DWT) technique is adopted in this study for the analysis of the wind speed data.

3.2.1 Detrending process

According to Fig. 2(a), the 10 min mean wind speed during the whole storm varies significantly at each height. Such time-varying mean wind speed occupies very low frequency range (corresponding frequency range of the 10 min sampling interval signal is [0, 1/1200] Hz). The variation of mean wind speed is known as macro-meteorological variation. The long term observation of this low frequency variation can be used for estimation of design mean wind speed in structural design. However, it is usually not taken into accounts when wind induced response of structure is calculated.

For the wind speed analyzed in this study, to remove the low frequency component whose period is approximately 10 min, 13-level decomposition with "Daubechies wavelets" is applied (Daubechies 1992). DWT uses a couple of filters—high pass and low pass filters—to decompose the input signal into two components, each of them occupies half band of the original frequency range, named the approximate coefficients (low frequency sub-band) and detail coefficients (high frequency sub-band).

The trend $U_{tr}(t)$ which corresponds to the approximate component of the 13th level within the frequency range of [0, 5×2^{-13}]Hz are subtracted from the original data. Fig. 3 shows the trend wind speed and the 10 min constant mean wind speeds at the 4 heights from the 6th hour to 10th hour. The detrending process can then be express in Eq. (5)

$$U_{dt}(t) = U(t) - U_{tr}(t) \tag{5}$$

where $U(t)$ is the original wind speed, $U_{dt}(t)$ is the detrended fluctuating wind speed, $U_{tr}(t)$ is the trend component.

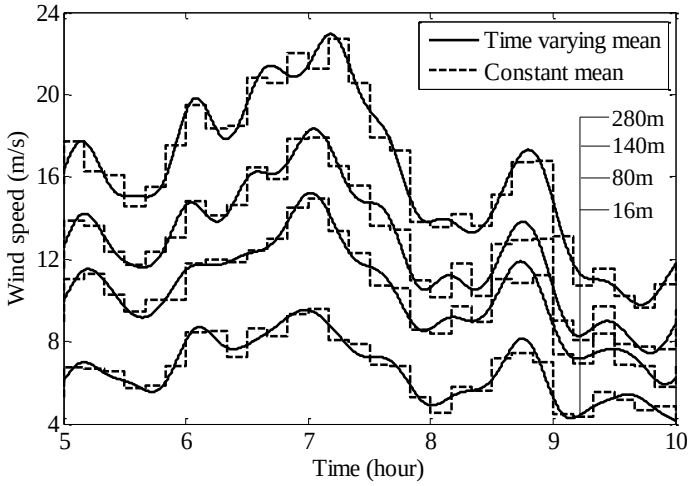

Fig. 3 Comparison of the trend and the 10 min mean wind speed

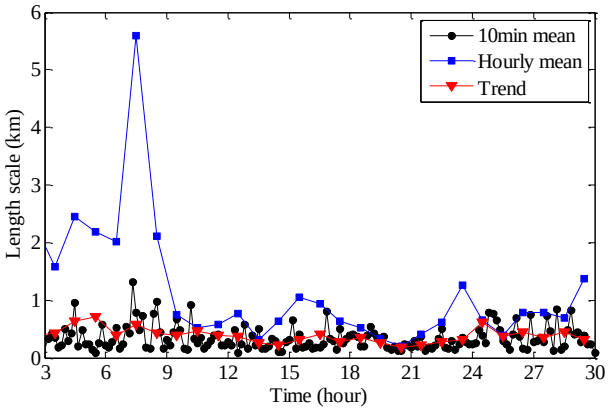

Fig. 4 Integral length scale at 280m high calculated by different methods

After the detrending process, Mann-Kendall test is applied again to the same time series tested in Sec. 3.1. The results show that 21 out of 27 1-hour samples are checked to have no trend indicating that the detrended data can mainly satisfy the constant mean assumption.

3.2.2 Application

One of the most direct applications of this detrending technique is to calculate the longitudinal integral length scale of wind, which is the most basic parameter for wind speed. Eq. (6) gives the traditional definition of the integral length scale based on the constant mean approach.

$$L = \frac{\overline{U}}{\sigma^2}\int_0^T R(t)dt \tag{6}$$

where σ^2 is the variance of fluctuating wind speed; T is the time period; $\overline{U}$ is the corresponding longitudinal mean wind speed; $R(t)$ is the auto-covariance function of the fluctuating longitudinal wind speed.

To calculate the integral length scale using Eq. (6), 10min records may not be long enough to get stable results. However, if 1-hour long records based on the constant mean approach are used, the low frequency trend component may severely distort the calculated results from the credible range. The wind records at 280 m high from 4th hour to 30th hour shown in Fig. 2 are selected to calculate the integral length scale. The results based on 10 min and 1-hour time intervals according to Eq. (6) are shown in Fig. 4. Although the results based on 10 min time interval are more reliable but they are quite unstable.

If the wind speeds data are pre-processed by the detrending technique, and Eq. (6) can be modified as

$$L = \frac{\overline{U}}{\sigma_{dt}^2}\int_0^T R_{dt}(t)dt \tag{7}$$

where σ_{dt}^2 is the variance of fluctuating wind speed $U_{dt}(t)$, $R_{dt}(t)$ is the auto-covariance function of $U_{dt}(t)$.

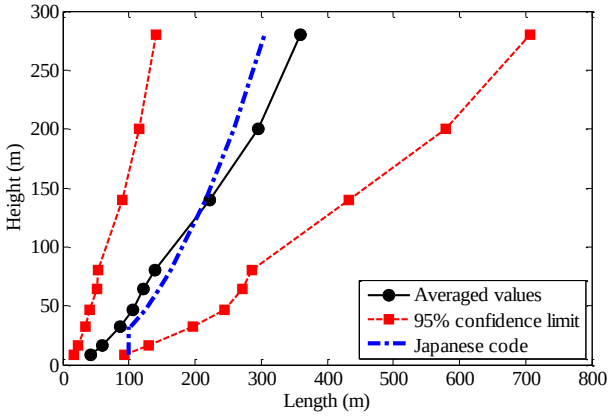

Fig. 5 Profile of integral scale based on the detrended wind speed

As shown in Fig. 4, the results after detrending are much more stable than that based on 10 min long records, and much more reliable than that based on the original 1-hour long data.

Fig. 5 shows the integral length scales at nine heights obtained based on the records of 44 synoptic storms. Totally 799 1-hour samples are adopted for the statistics at each height. The results are compared with the values recommended in Japanese Code (AIJ 2004). The averaged length scale at each height can be checked very close to the values recommended in Japanese Code. The upper and lower 95% confidence limits are also shown Fig. 5, where 95% confidence limit means that there are 5% of observed integral length scales are higher (smaller) than the upper(lower) limit.

4. Further discussion on fluctuating component

After subtracting the low frequency trend component from the original data, the trend induced non-stationarity is basically removed. Thus, the probability density distribution of the detrended data is checked.

Fig. 6 shows the probability density distribution of the 6th hour's $U_{dt}(t)$ at 280 m high. $U_{dt}(t)$ can be checked does not follow Gaussian distribution with obviously negative skewness. Such results clearly indicate that the Gaussian distribution assumption to the fluctuating wind speeds are not valid. Thus, the non-Gaussian property will be further investigated in this study.

4.1 Skewness analysis

The skewness of 1-hour fluctuating wind speeds from 4th to 30th hour at 16 m, 80 m, 140 m, and 280 m are shown in Fig. 7(a). Most of results can be checked having non-zero skewness values. That is to say the longitudinal fluctuating wind speeds are mostly non-Gaussian, which is different from the widely used assumption. By averaging every hour's skewness value from the 4th to 30th hour for data from every measuring point, the averaged values are plotted with corresponding height (as shown in Fig. 7(b)), the skewness tends to gradually decrease from positive to negative when altitude increases.

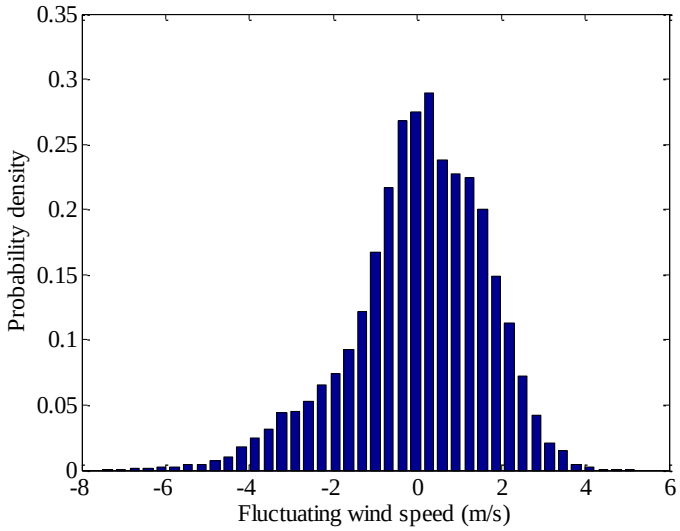

Fig. 6 Probability distribution of 6th hour's detrended fluctuating wind speeds at 280 m

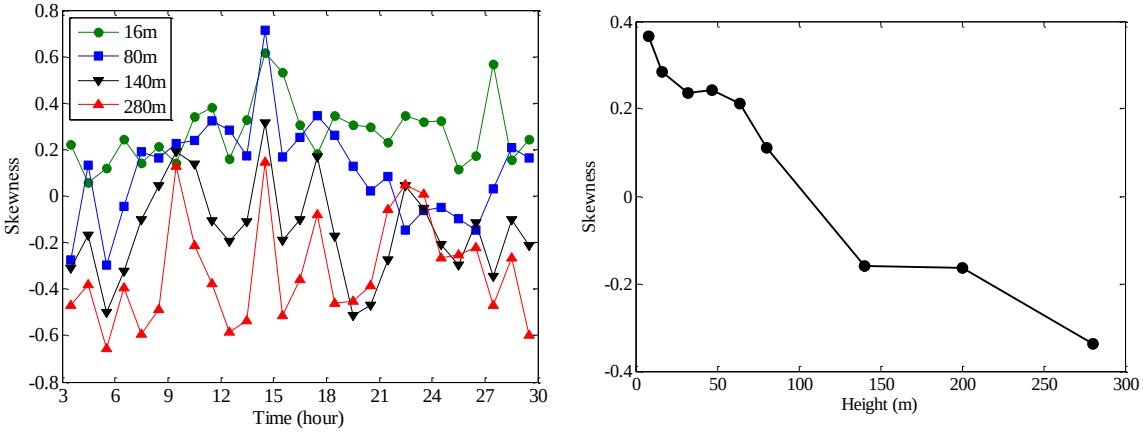

(a)Skewness of detrended wind speeds of each hour at four heights

(b) Averaged skewness values of fluctuating wind speed at every height

Fig. 7 Skewness of fluctuating wind speeds

To find the causes of the non-zero skewness, 13 levels' detail components of the decomposed wind speed with the i^{th} level occupies $[5\times2^{-i}, 5\times2^{-(i-1)}]$Hz are studied. For every hour's data, the decomposed detail component is subtracted from $U_{dt}(t)$ level by level from low frequency to high frequency to examine their effects on the skewness. The components that are mostly responsible to the skewness of distribution are finally removed, leaving the remaining components symmetrically distributed. This process is named as the de-skewness process.

Fig. 8(a) shows the component of the 6^{th} hour's $U_{dt}(t)$ at 280 m that leads to negative skewness of the fluctuating wind speeds' distribution. The frequency range of it is $[5\times2^{-13}, 5\times2^{-8}]$Hz. Fig. 8(b)

shows probability distribution of the remaining component of $U_{dt}(t)$, which is much more symmetric than that shown in Fig. 6 with the skewness of 0.02.

Same procedure is applied to all the fluctuating wind speeds $U_{dt}(t)$ at the four heights. The components that occupy the low frequency range are found to be largely responsible for the skewness of fluctuating wind speeds. Based on such observation, the detrended wind speeds can thus be further separated into the high and low frequency components as

$$U_{dt}(t) = U_H(t) + U_L(t) \tag{8}$$

where $U_H(t)$ and $U_L(t)$ are the high frequency component and the low frequency component of the $U_{dt}(t)$ respectively. A detailed analysis for the asymmetric distribution of fluctuating wind will be further discussed in this study.

For the storm being analyzed in this study, $U_L(t)$ are approximately in the range of $[5\times2^{-13}, 5\times2^{-9}]$Hz at 16 m and 80 m high, and within $[5\times2^{-13}, 5\times2^{-8}]$Hz at 140 m and 280 m high. Fig. 9 shows the skewness of the wind speeds after the de-skewness process, it can be checked that after the de-skewness process, the retained components become much more symmetrically distributed at every height comparing with the detrended fluctuating wind speeds.

4.2 Kurtosis analysis

According to the probability density shown in Fig. 8(b), although $U_H(t)$ is symmetrically distributed, it is still a non-Gaussian process. In comparing with the fitted Gaussian distribution, it is clear that the fourth moment of the distribution—kurtosis, which reflects the sharpness of the distribution, is much higher than Gaussian distribution. For an exact Gaussian distribution, the kurtosis value is 3.0.

In light of this example, kurtosis of all the retained $U_H(t)$ at the four heights are examined for every hour and the results are shown Fig. 10. Most of the kurtosis values are found to be higher than 3.0 and quite unstable, which indicates that the $U_H(t)$ is still a non-Gaussian distribution. In this study, the reason of this high kurtosis will be further investigated.

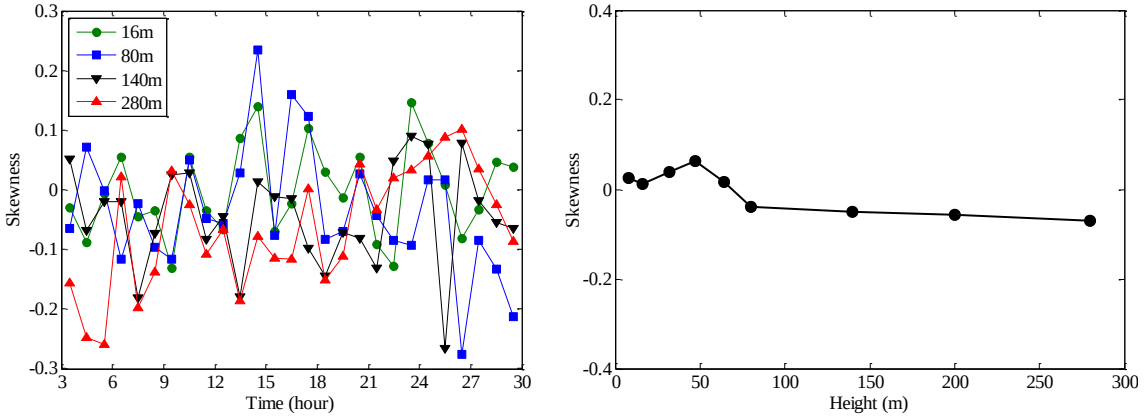

(a)Skewness of de-skewed wind speeds of each hour at four heights

(b) Averaged skewness values of de-skewed wind speed at every height

Fig. 9 Skewness of de-skewnessed wind speeds

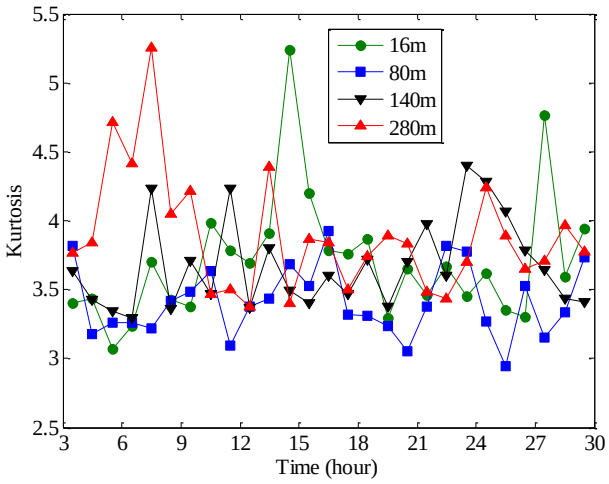

Fig. 10 Kurtosis of de-skewnessed wind speeds of each hour at four heights

5. Mechanisms of non-Gaussianity

Based on the previous analysis in Sec. 4, the detrended fluctuating wind speed $U_{dt}(t)$ are found to be asymmetrically distributed, and the high frequency component $U_H(t)$ are sharply distributed which leads to the high kurtosis. It is still interesting to find out what is the underlying mechanism that causes the asymmetrical distribution of $U_{dt}(t)$ and high kurtosis in high-frequency band. Thus, the fluctuating wind speeds are further studied by decomposing time series into monocomponents. Maximal-Overlap Discrete Wavelet Package Transform (MODWPT) (Olhede and Walden 2004) is applied in this analysis. MODWPT is a version of wavelet transform that does away with the downsampling step. Thus it ensures the important property of circular shift equivariance. Another merit of MODWPT is it can partition the frequency axis into 2^j equal with frequency bands at jth level of transformation, so that it makes the transformation give better frequency resolution. Then the instantaneous phase and amplitude of each monocomponent are estimated based on the Direct Quadrature (DQ) method, which is an improved method of Hilbert transform developed by Huang, Wu *et al*. (2009). The instantaneous phase and amplitude can provide important information of the random process for analysis.

The 6th hour's longitudinal wind speeds at 280 m high is decomposed into the 13th level by adopting MODWPT technique, which means the frequency is partitioned into 2^{13} equal width bands from 0 to 5 Hz, and instantaneous amplitude—$A(f, t)$ and phase—$\phi(f, t)$ of every monocomponent are obtained based on DQ method. And the monocomponent at frequency f—$V(f, t)$ can be expressed as

$$V(f,t) = A(f,t) \times \cos(\phi(f,t)) \tag{9}$$

Based on the instantaneous amplitudes, the instantaneous energy of frequency "f", and time "t" is obtained as follows

$$P(f,t)=\frac{A^2(f,t)}{\Delta f} \tag{10}$$

where Δf is the band width of corresponded monocomponent. $P(f, t)$ are then plotted in time-frequency domain as shown in Fig. 11. The corresponding $U_{dt}(t)$ is also given on the top of the diagram as a reference. This figure clearly depicts the non-stationary essence of the fluctuating wind, where energy of every frequency varies with time. Based on the spectrum in time-frequency domain, the mean energy of each frequency in time domain can also be calculated

$$\overline{P}(f)=\frac{1}{T}\int_0^T P(f,t)dt \tag{11}$$

The mean energy is used to compare with the power spectrum which is calculated by the traditional Fourier transform method. Fig. 12 shows the Power Spectrum Density (PSD) based on the two methods. Von Karman spectrum which is a widely accepted PSD model of fluctuating wind speed in structure engineering field is also plotted in Fig. 12. The two PSD obtained by different methods are almost identical and both of them match well with Von Karman spectrum.

This comparison indicates that the time-frequency analysis used in this study is a valid analyzing method. This results also confirm that although the wind speed has time varying energy as shown in Fig. 11, the hourly averaged values at every frequency conform to the classical Von Karman model, which suggests that the fluctuating wind speeds is a weakly-stationary process.

In the following part of this section, the causes of skewness and high kurtosis will be discussed from the phase, amplitude and energy point of view of the decomposed monocomoponents.

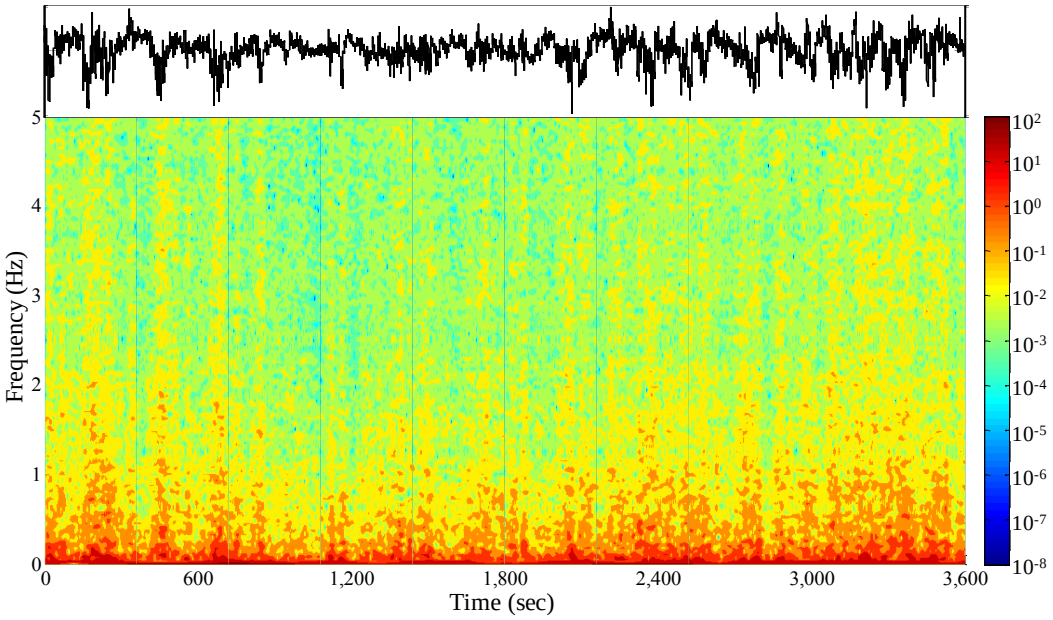

Fig. 11 Energy distribution of fluctuating wind speed in time-frequency domain

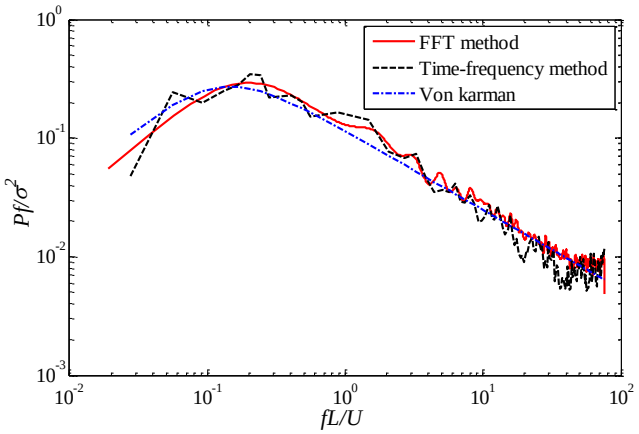

Fig. 12 Power spectrum of fluctuating wind speed by different methods

5.1 Property of $U_L(t)$

Based on the study in Sec. 4.1, $U_L(t)$ shows clear relation with the skewness of the distribution. Fig. 13(a) shows the instantaneous amplitude and phase of the decomposed monocomponent of the 6th hour's data at 280 m, which mainly occupies the [5×2^{-12}, 7.5×2^{-12}]Hz frequency band. As the effects of phase need be checked, the following modification to original values will be made

$$\tilde{V}(f,t) = A(f,t)\times\cos(\tilde{\phi}(f,t)) \tag{12}$$

and

$$\tilde{\phi}(f,t) = \phi(f,t) + \alpha, \tag{13}$$

where $A(f, t)$ and $\phi(f, t)$ are the amplitude and phase of the original $V(f, t)$, α is a random value that follows uniform distribution [$-\pi$, π]. This is actually a phase shifting operation. The effects of phase shifting are shown in Fig. 13(b).

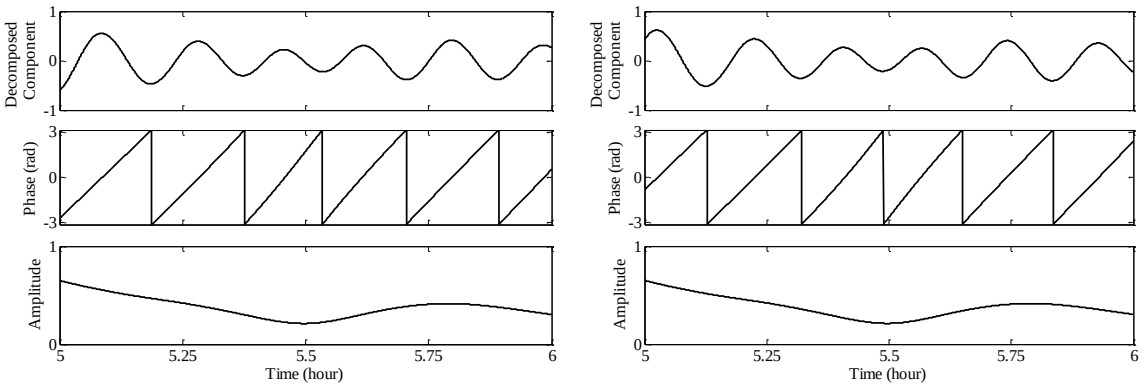

(a) Original decomposed monocomponent (b) Phase shifted decomposed monocomponent

Fig. 13 Phase and Amplitude of the decomposed monocomponent.

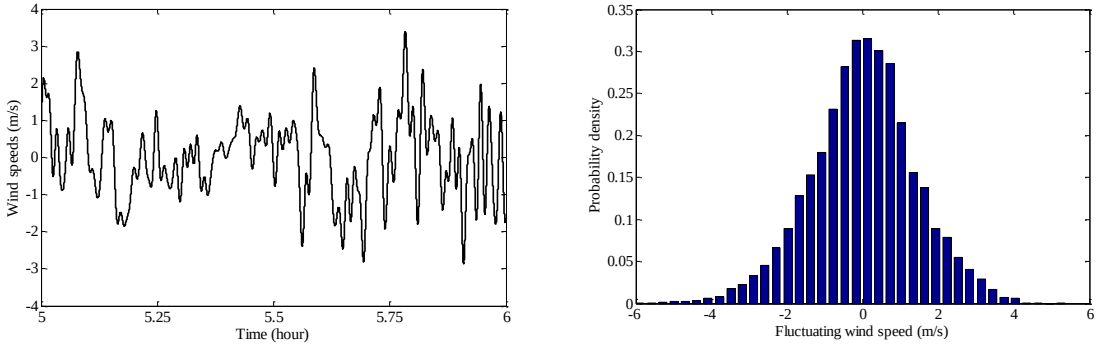

(a) Time series of modified $U_L(t)$ (b) Probability density distribution of modified $U_{dt}(t)$

Fig. 14 Effects of phase shuffling to fluctuating wind speed.

By applying the same operation to every monocomponent of $U_L(t)$, the original combination of phases among different frequency bands are shuffled. Fig. 14(a) shows one realization, which is the phase shuffled $U_L(t)$ of 6th hour fluctuating wind speeds at 280 m. Comparing with Fig. 8(a), the modified $U_L(t)$ are more symmetrically distributed around zero. $U_H(t)$ and the modified $U_L(t)$ can be reconstructed into a modified $U_{dt}(t)$. Fig. 14(b) shows probability density distribution of modified $U_{dt}(t)$. Comparing with Fig. 6, the distribution becomes much symmetric than the original one. In this procedure, since the phase of every monocomponent is randomly shifted, Monte Carlo method is adopted in order to get statistics of a large number of trials (totally 2000 trials are examined in this case). The skewness of every modified version of $U_{dt}(t)$ are calculated, with the mean and standard deviation of -0.08 and 0.17, respectively. Such results indicate that once such combination is broken, the skewed distribution of wind speed disappears consequently. And the phase combination of monocomponents of $U_L(t)$ directly determines the characteristics of the fluctuating wind.

The effect of amplitude can also be checked. The time varying amplitudes in each frequency band is replaced by a constant value

$$\overline{A}(f) = (\frac{1}{T}\int_0^T P(f,t)dt)^{0.5} \tag{14}$$

which also insures the total energy within every frequency band is unchanged. The modified monocomponent becomes

$$\overline{V}(f,t) = \overline{A}(f) \times \cos(\phi(f,t)) \tag{15}$$

This procedure is named as energy normalization. Fig. 15(a) is the time series of $U_L(t)$ after normalizing energy. The wind speed is then reconstructed by combining $U_H(t)$ and the energy normalized $U_L(t)$. Fig. 15(b) shows the probability density distribution of the modified $U_{dt}(t)$. It is clear that the skewness is still very high.

The above analysis indicates that the monocomponents decomposed from $U_L(t)$ possess a specific combination of instantaneous phase, which can lead to the asymmetric fluctuation of $U_L(t)$,

and subsequently affect the skewness of probability density distribution of $U_{dt}(t)$. The time varying energy, however, does not show strong effects.

5.2 Property of $U_H(t)$

The reason of high kurtosis of $U_H(t)$ is studied through similar manner as $U_L(t)$. The phase effect is also studied by the means of phase shifting operation to every monocomponent, according to Eqs. (12) and (13). The modified $U_H(t)$ are then reconstructed. Monte Carlo method is again adopted to investigate the effect of phase, and the kurtosis of every $U_H(t)$ is calculated. The mean kurtosis is 3.97, which is still much higher than 3.0, although it is smaller than the original value which is 4.45. Meanwhile the skewness values of all the modified $U_H(t)$ have a mean of 0.0, with standard deviation 0.08. These results indicate that although phase does not show strong effects on the kurtosis of distribution, and almost has no effect on the skewness.

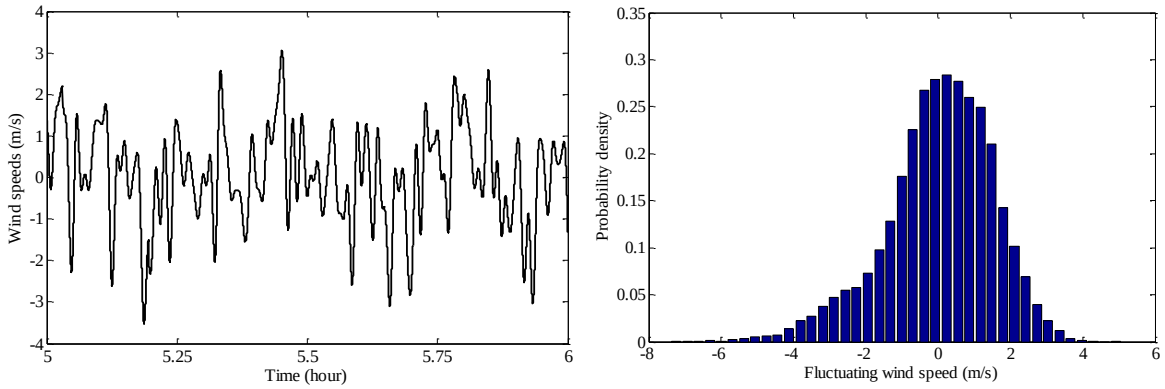

(a) Time series of modified $U_L(t)$ (b) Probability density distribution of modified $U_{dt}(t)$

Fig. 15 Effects of energy normalization to fluctuating wind speed

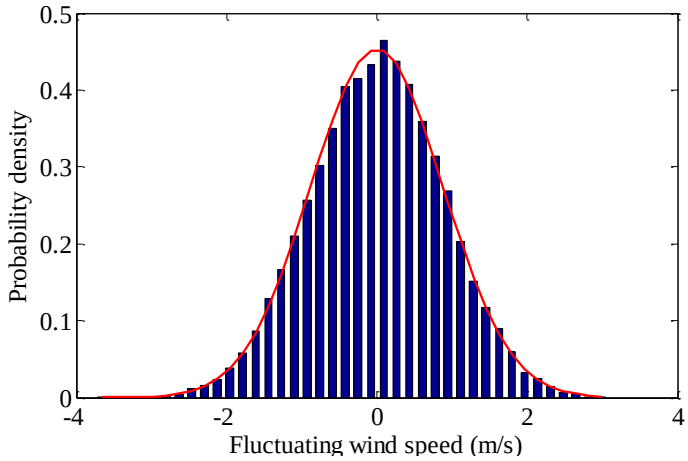

Fig. 16 Probability density distribution of energy normalized $U_H(t)$

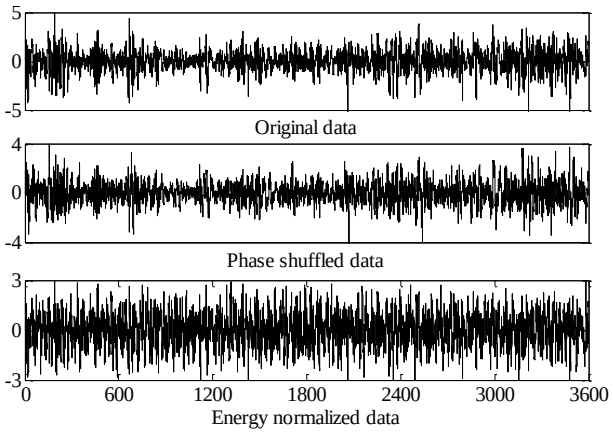

Fig. 17 Different versions of time series $U_H(t)$

The effects of time varying amplitude is also studied. The instantaneous energy of every monocomponent of $U_H(t)$ is normalized according to Eq. (16), and $U_H(t)$ is reconstructed by superposing all the energy normalized monocomponents. The distribution of energy normalized $U_H(t)$ is shown in Fig. 16, with the kurtosis 2.91. The red line in Fig. 16 is the fitted Gaussian distribution, which can match the distribution quite well.

Fig. 17 shows three time series, the first one is the original $U_H(t)$, the second is the phase shuffled version, and the last one is the energy normalized version. Results shown in Fig. 17 also indicate that comparing with phase, time varying energy has much stronger effects on distribution property. After energy normalization, $U_H(t)$ becomes much more stationary along time than the original one, and this stationarity also leads the process to be Gaussian.

The time varying energy of $U_L(t)$ can be physically interpreted as the intermittency of small-scale eddies of wind. Some existing studies (Yamada and Ohkitani 1991, Dubrulle 1994) have claimed that this intermittency is caused by the inconsistent transmission of turbulence energy from large scale eddies to the small scales.

5.3 Dependence between $U_L(t)$ and $U_H(t)$

As known that the energy of small scale eddies is cascaded from large scale eddies (She and Leveque 1994). Therefore, based on the observed wind speeds data at various heights from 8 m-280 m, analysis can be made to check the dependence between the low frequency components ($U_L(t)$) and the high frequency components($U_H(t)$) from the data point of view. Also, if the such dependence can further affect the non-Gaussian property of $U_{dt}(t)$ will be examined.

Fig. 18 shows the time-series of fluctuating wind speed of $U_L(t)$ and corresponding time varying turbulence energy of $U_H(t)$ in the same diagram. One hour long data from both 280 m and 8m are shown in Fig. 18. It can be clearly seen from Fig. 18(a) that strong turbulence always occurs at the moment that $U_L(t)$ has large negative values. That means the two variables are actually negatively correlated. While as shown in Fig. 18(b), the two variables from the data at 8m high show the positive correlations. Such results indicate that although the $U_L(t)$ and $U_H(t)$ themselves are theoretically uncorrelated because they occupy different frequency band, time

varying turbulence energy of $U_H(t)$ clearly depends on $U_L(t)$. For further investigations, the correlation coefficients between $U_L(t)$ and time varying turbulence of $U_H(t)$ are calculated for every hour's data from all the 9 measuring heights.

In order to examine if such dependence may also be a reason that leads to different skewness of fluctuating wind speeds, the obtained correlation coefficients are plotted with corresponding skewness values of every hour's fluctuating wind speed as shown in Fig. 19. Results belonging to different heights are indicated by different labels in the figure. Clear linear relations between the two variables can be observed, which indicates that the dependence between $U_L(t)$ and $U_H(t)$ is also a factor that affects the skewness of probability density distribution of $U_{dt}(t)$. Meanwhile, with the skewness of $U_{dt}(t)$ decreasing from positive to negative gradually with the increase of heights, the correlation coefficients also shift from positive to negative accordingly. Such results also conform with the observation in Fig. 18, implying that in high altitude(>100 m) the turbulence energy is more likely to be transmitted to small scale eddies when $U_L(t)$ has large negative values, and in the low altitude(<100 m) opposite phenomenon is more likely to be observed.

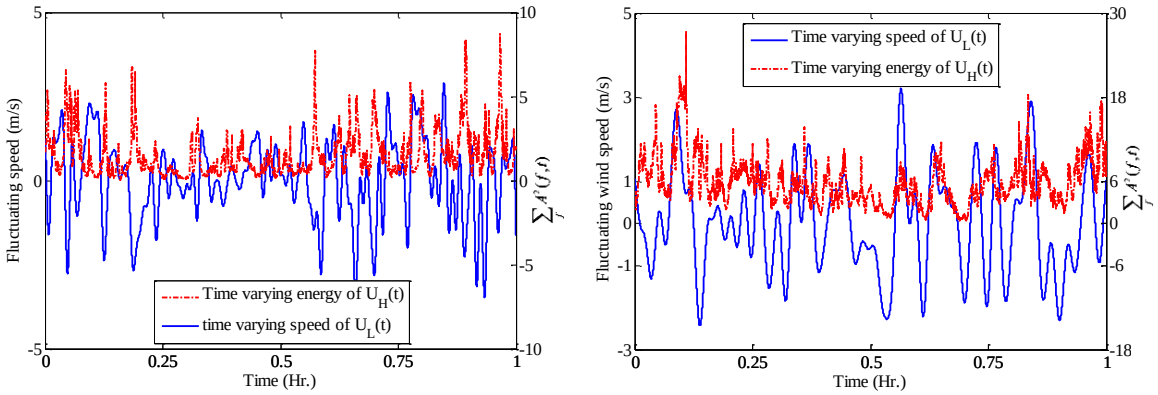

(a) 280 m (b) 8 m

Fig. 18 Dependence check between $U_L(t)$ and $U_H(t)$

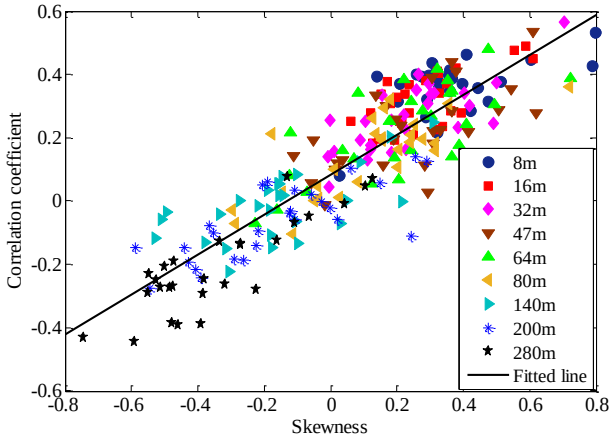

Fig. 19 Skewness vs. Correlation coefficient at all measuring heights

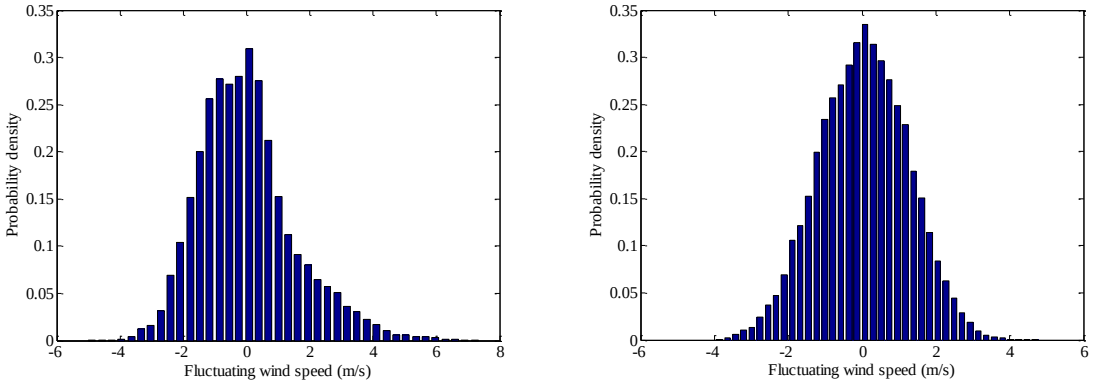

(a) Phase shifted by π (b) Phase shuffled

Fig. 20 Probability density distribution of modified $U_{dt}(t)$

5.4 Examination of Non-Gaussianity of fluctuating wind speed through fourier transform

In previous part of this section, the fluctuating wind speed is studied in details by the means of wavelet transform which is a typical tool used for non-stationary process. Based on previous study, it is known that the fluctuating wind speed does not show strong non-stationarity, it is more likely to be a weakly-stationary process. Thus, the Fourier transform is adopted here to study the non-Gaussian property.

In this case, only the effect of phase can be checked, as the amplitude is constant for the component at each frequency after Fourier transform. The effects of phase is studied by firstly mapping the data into frequency domain through Fourier transform, then the phase of the data are modified, finally the modified data are mapped back to time domain through inverse Fourier transform. Therefore, the effect of phase can be observed by comparing the data before and after the modification.

The 6th hour's fluctuating wind speed data are still adopted for illustration. Fig. 20(a) shows the probability density distribution of the data by shifting phases of all component by π. Comparing with Fig. 6, it clearly shows that distribution are reversed, which means the skewness of the modified process becomes opposite as the original one. By shuffling the phase of component at each frequency, the probability density distribution becomes as shown in Fig. 20(b). One can see that the fluctuating wind speeds are almost symmetrically distributed after the phase shuffling. From the results shown in Fig. 20, the strong effects of phase on the distribution of fluctuating wind speeds can be checked clearly, which is similar as the results shown in Sec. 5.1. While due to the limitation of Fourier transform, the effect of time varying amplitude cannot be studied.

6. Conclusions

Non-Stationarity and non-Gaussian property are two of the most important features of wind speed. In this study, the two properties are studied based on the time-frequency analyzing tool. The wind speeds recorded from the Beijing 325 m high meteorological tower are used for the analysis.

The strongest synoptic wind storm from Nov., 2012 to Feb., 2014 is selected for the detailed analysis.

The data is firstly detrended by removing the very low frequency component as some existing methods. It is found that after the detrending procedure, some basic wind characteristics such as the integral length scale can be estimated more reasonably and more stable than the results obtained by simply subtracting the constant mean values. The integral length scales at different heights are then calculated based on the 1-year records, and the results are very close to the values recommended by Japanese code.

The probability distribution property is further checked based on the third and fourth moment of the detrended fluctuating wind speed. It is found that the low frequency component is mainly responsible to the skewness of distribution. The upper limit of the period of this component is about tens of seconds. For the high frequency component, although the probability distribution is symmetric, it is still non-Gaussian distributed with high kurtosis.

The non-Gaussian features are further studied by adopting the MODWPT technique. It is found that the detrended fluctuating wind speeds is weakly-stationary processes. Thus, the phase and the time varying energy's effects are checked respectively. Results show that the phases of different monocomponents in low frequency band can strongly affect the skewness of fluctuating wind. This results are also supported by the analysis through Fourier transform. And the time varying energy are more responsible to the high kurtosis of the high frequency component. The dependence between low frequency component and high frequency component of the fluctuating wind speed is also studied, results show that the dependence is also a factor of causing the asymmetric distribution of fluctuating wind.

Acknowledgements

This study is supported by the National Natural Science Foundation of China (51408207) and the 111 Project on Grant B13002. Support is also given by the Key laboratory of bridge wind resistant and new technology of Hunan province (15K028). The authors give special thanks to Prof. S.S. Law and Prof. X.Z. Chen for their great help.

References

Architectural Institute of Japan (2004), Chapter 6: Wind Loads, Recommendations for Loads on Buildings.

Balderrama, J.A., Masters, F.J. and Gurley, K.R. (2012), "Peak factor estimation in hurricane surface winds", *J. Wind Eng. Ind. Aerod.*, **102**, 1-13.

Chen, L. and Letchford, C.W. (2005), "Proper orthogonal decomposition of two vertical profiles of full-scale nonstationary downburst wind speeds", *J. Wind Eng. Ind. Aerod.*, **93**, 187-216.

Chui, C.K. (1992), *An Introduction to Wavelets*, Academic Press, INC.

Daubechies, I. (1992), Ten Lectures on Wavelets, SIAM, Philadelphia, PA.

Dubrulle, B. (1994), "Intermittency in fully developed turbulence: Log-poisson statistics and generalized scale covariance", *Phys. Rev. Lett.*, **73**(7), 959-962.

Farge, M. (1992), "Wavelet transforms and their applications to turbulence", *Annu. Rev. Fluid Mech.*, **24**(1), 395-458.

Gong, K. and Chen, X. (2014), "Influence of non-Gaussian wind characteristics on wind turbine extreme response", *Eng. Struct.*, **59**, 727-744.

Gurley, K.R. and Kareem, A. (1999), "Applications of wavelet transforms in earthquake, wind and ocean engineering", *Eng. Struct.*, **21**(2), 149-167.
Hahn, S.L. (1996), *Hilbert Transforms in Signal Processing*, Artech House, Inc., Boston, London.
Hamed, K.H. and Rao, A.R. (1998), "A modified Mann-Kendall trend test for auto correlated dat", *J. Hydrol.*, **204**, 182-196.
Hayashi, T. (1994), "An analysis of wind velocity fluctuations in the atmospheric surface layer using an orthogonal wavelet transform", *Bound.-Lay. Meteorol.*, **70**(3), 307-326.
Hu, L., Xu, Y.L. and Huang, W.F. (2013), "Typhoon-induced non-stationary buffeting response of long-span bridges in complex terrain", *Eng. Struct.*, **57**, 406-415.
Huang, M.F., Huang, S., Feng, H. and Lou, W. (2016), "Non-Gaussian time-dependent statistics of wind pressure processes on a roof structure", *Wind Struct.*, **23**(4), 275-300.
Huang, N.E., Wu, Z., Long, S.R. and Arnold, K.C. (2009), "On instantaneous frequency", *Adv. Adapt. Data Anal.*, **1**(2) 177-229.
Hui, M.C.H., Larsen, A. and Xiang, H.F. (2009), "Wind turbulence characteristics study at the Stonecutters Bridge site: Part I—Mean wind and turbulence intensities", *J. Wind Eng. Ind. Aerod.*, **97**, 22-36.
Hui, M.C.H., Larsen, A. and Xiang, H.F. (2009), "Wind turbulence characteristics study at the Stonecutters Bridge site: Part II: Wind power spectra, integral length scales and coherences", *J. Wind Eng. Ind. Aerod.*, **97**, 48-59.
Kareem, A. (2008), "Numerical simulation of wind effects: A probabilistic perspective", *J. Wind Eng. Ind. Aerod.*, **96**, 1472-1497.
Kareem, A. and Kijewski, T. (2002), "Time-frequency analysis of wind effects on structures", *J. Wind Eng. Ind. Aerod.*, **90**, 1435-1452.
Kawai. H. (2009), "Importance of phase characteristics to pressure fluctuation", *Proceedings of the 7th Asia-Pacific Conf. on Wind Eng.* (APCWE VII), Taipei, Taiwan.
Kitagawa, T. and Nomura, T. (2003), "A wavelet-based method to generate artificial wind fluctuation data", *J. Wind Eng. Ind. Aerod.*, **91**, 943-964.
Li, Q.S., Xiao, Y.Q. and Wong, C.K. (2005), "Full-scale monitoring of typhoon effects on super tall buildings", *J. Fluid. Struct.*, **20**, 697=717.
Li, Q.S., Zhi, L.H. and Hu, F. (2010), "Boundary layer wind structure from observations on a 325 m tower", *J. Wind Eng. Ind. Aerod.*, **98**, 818-832.
McCullough, M., Kwon, D.K., Kareem, A. and Wang, L. (2014), "Efficacy of averaging interval for nonstationary winds", *J. Eng. Mech. - ASCE*, **140**(1), 1-19.
National Research Council (2005), National building code of Canada, Ottawa.
Olhede, S. and Walden, A.T. (2004), "The Hilbert spectrum via wavelet projections", *P. R. Soc. London A.*, **460**, 955-975.
She, Z. and Leveque, E. (1994), "Universal scaling laws in fully developed turbulence", *Phys. Rev. Lett.*, **72**, 336-339.
Su, Y. and Huang, G. and Xu. Y.L. (2015), "Derivation of time-varying mean for non-stationary downburst winds", *J. Wind Eng. Ind. Aerod.*, **141**, 39-48.
Tao, T., Wang H. and Li, A. (2016), "Stationary and nonstationary analysis on the wind characteristics of a tropical storm", *Smart Struct Syst.*, **17**(6), 1067-1085
Toriumi, R., Katsuchi, H. and Furuya, N. (2000), "A study on spatial correlation of natural wind", *J. Wind Eng. Ind. Aerod.*, **87**, 203-216.
Wang, L., McCullough, M. and Kareem, A. (2013), "Data-driven approach for simulation of full-scale downburst wind speeds", *J. Wind Eng. Ind. Aerod.*, **123**, 171-190.
Xu, Y.L. and Chen, J. (2004), "Characterizing nonstationary wind speed using empirical mode decomposition", *J. Struct. Eng. - ASCE*, **130**, 921-920.
Yamada, M. and Ohkitani, K. (1991), "Orthonormal wavelet analysis of turbulence", *Fluid Dyn. Res.*, **8**, 101-115.
Yi, J., Zhang, J.W. and Li, Q.S. (2013), "Dynamic characteristics and wind-induced responses of a super-tall building during typhoons", *J. Wind Eng. Ind. Aerod.*, **121**, 116-130.

CC